Eur. Phys. J A **2**, 157–171 (1998)

THE EUROPEAN PHYSICAL JOURNAL A

High spin structure study of the light Odd-A $f_{7/2}$ nuclei: ^{45}Sc, ^{45}Ti and ^{43}Ca

P. Bednarczyk[1], J. Styczeń[1], R. Broda[1], M. Lach[1], W. Męczyński[1], D. Bazzacco[2], F. Brandolini[2], G. de Angelis[3], S. Lunardi[2], L. Müller[2], N.H. Medina[2], D.R. Napoli[3], C.M. Petrache[2], C. Rossi Alvarez[2], F. Scarlassara[b], G.F. Segato[2], C. Signorini[2], F. Soramel[4]

[1] The Henryk Niewodniczański Institute of Nuclear Physics, PL-31342 Kraków, Poland
[2] Dipartimento di Fisica dell'Universita and INFN, I-35131 Padova, Italy
[3] INFN, Laboratori Nazionali di Legnaro, I-35020 Legnaro, Italy
[4] Dipartimento di Fisica dell'Universita and INFN, I-33100 Udine, Italy

Received: 27 October 1997 / Revised version: 29 December 1997
Communicated by B. Herskind

Abstract. High-spin states in ^{45}Sc, ^{45}Ti and ^{43}Ca were studied by means of multiple γ- and γ-recoil-coincidences with the use of the GASP array and the Recoil Mass Spectrometer. The nuclei were populated in the 60 MeV ^{18}O + ^{30}Si reaction. For the DSAM lifetime measurement the ^{35}Cl + ^{12}C reversed kinematics reaction was used. In the article, a complete description of the experimental techniques used in course of the performed experiments is presented. The level schemes and the detailed information on the observed state properties, including B(M1) and B(E2) transition rates are inserted as well as their shell model interpretation.

PACS. 27.40+z $39 \leq A \leq 58$ – 21.10.Tg Lifetimes – 21.60.Cs Shell model – 21.60.Ev Collective models

1 Introduction

Although the $f_{7/2}$ nuclei lie in a relatively narrow region between the doubly magic spherical nuclei ^{40}Ca, ^{48}Ca and ^{56}Ni, several of their properties can be viewed as signs of collectivity. In particular, in the odd isotopes of Ca, Sc, Ti or V the levels with $K^\pi = 3/2^+$ form regular rotational-like bands [1–8]. The lifetime data available for the low lying states [2] point out that the E2 transition rates between the levels belonging to the bands are significantly enhanced with respect to the single particle estimates. This effect was related to the collective rotation of the nucleus with positive deformation of $\beta \approx 0.25$ [3]. Moreover, in the middle of the $f_{7/2}$ shell the ^{48}Cr nucleus exhibits collective features with a rotational band which, however, seems to terminate when the $f_{7/2}$-shell protons and neutrons are fully aligned [9].

It turns out that the collective features of the $f_{7/2}$ nuclei as band like structures and strong in-band E2 transition rates emerge when shell model calculations are performed within the extended configuration space [10]. As was also shown in [11] where the case of ^{48}Cr is discussed, the interaction between nucleons from fp-orbitals gives rise to a prolate deformed nuclear shape with almost constant value of the intrinsic quadrupole moment.

The shell model calculations performed so far for the odd-A $f_{7/2}$ nuclei have been in most cases restricted to the levels with natural i.e. negative parity. On the other hand, for the discussion on the origin of the nuclear deformation in these nuclei – states resulting from the core excitations are relevant. In order to take into account even very simple core excitation as $d_{3/2}$ proton or neutron hole quasiparticle, one has to deal with a significant extension of the shell model configuration space. Nevertheless, the present computational techniques and newly available sets of effective interactions coupling the states from sd and fp orbitals [12] make such calculations feasible.

In the $f_{7/2}$ shell nuclei the experimental knowledge about the structure of high spin states which result from an excitation to the orbitals located above the $f_{7/2}$ shell is still scarce. In those nuclei only in few cases the states with angular momentum greater than the maximum aligned spin $J_{\max} = [1/2(Z-20)(28-Z) + (N-20)(28-N)]$ available for the $f_{7/2}^{A-40}$ configuration have been observed [13, 14]. Therefore, the experimental investigations of levels with $J > J_{\max}$ are of great importance to learn more on the effective interactions across the shells and to study the band termination effects.

Two main experimental difficulties have limited the information on the high spin states in the $f_{7/2}$ shell nuclei. The high energies of γ-ray transitions which generally occur between such states imply short lifetimes of those states and cause an excessive Doppler shift and broadening of measured γ-lines. Secondly, the available target/projectile and projectile energy combinations limit the angular momentum to be transferred to the compound nucleus to less than 40 ħ. Hence, the population of the high spin states (say $J > 10\,\hbar$) in a certain residual nucleus competes with many stronger reaction channels. Only the new experimental facilities such as multidetector arrays and recoil mass spectrometers, due to their enhanced sensitivity and selectivity offer an excellent opportunity to study high spin excitations in the $f_{7/2}$ nuclei.

In the present study, we have focused our interest on the high-spin structure ($J > J_{\max}$) of the $f_{7/2}$ nuclei: ^{43}Ca, ^{45}Sc and ^{45}Ti, where the quasi-rotational intruder bands develop already at low angular momenta [5–7].

Some of the results have been partially reported previously together with a theoretical interpretation [15–18]. In the present paper a full description of the experiments, with special emphasis on the lifetime measurements by using the Doppler Shift Attenuation Method (DSAM), and a detailed discussion of the results are given.

2 Experiments and data analysis

The various experiments described in this work have been performed at the XTU Tandem accelerator of the Laboratori Nazionali di Legnaro.

In the following sub-sections details of the experiments and the subsequent data analysis are given.

2.1 Pilot measurement

Our study of nuclei around mass A = 45 was initiated through a "pilot measurement" by using the fusion evaporation reactions induced by 55 MeV and 65 MeV ^{18}O beams bombarding a thin 220 mg/cm^2 ^{30}Si target evaporated on 30 mg/cm^2 carbon foil. One of the purposes was to learn if one could gain in angular momentum transfer by increasing the bombarding energy in spite of loosing efficiency for a given evaporation residuum due to higher number of competing channels.

To measure γ-rays we employed four 20% Compton shielded Ge detectors placed at a distance of 15 cm from the target, positioned at 45° and 135° with respect to the beam axis. The recoils were separated by the Recoil Mass Spectrometer (RMS) [19] and identified in the focal plane detector consisting of a Parallel Plate Avalanche Counter (PPAC).

The cathode of the multiwire chamber provided a trigger signal which enabled the acquisition. The collected events incorporated γ-ray energy, horizontal (X) and vertical (Y) position of the recoil in the RMS focal plane, and its time of flight through the spectrometer (TOF). The mass of the recoil was identified by the X position whereas the Y and the TOF parameters served to exclude scattered primary beam nuclei.

In this experiment, we focused in particular on the ^{45}Sc and ^{45}Ti nuclei. The energy corresponding to the maximum cross-section predicted by the CASCADE code [20] calculations (to be approximately the same for the reaction channels: ^{30}Si(^{18}O,p2n)^{45}Sc and ^{30}Si(^{18}O,2pn)^{45}Ti) was exceeded by 15 MeV and 25 MeV, respectively, for the two applied beam energies used in the experiment. The measured and calculated by CASCADE mass distributions in the compound nucleus decay are shown in Fig. 1.

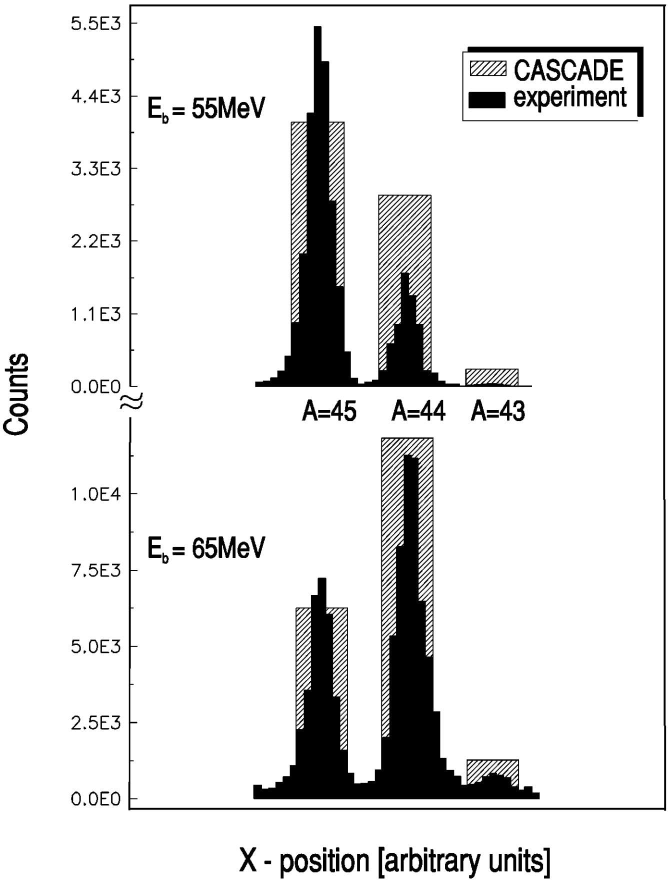

Fig. 1. Evaporation residua mass distribution measured and calculated with the CASCADE code for the 55, 65 MeV ^{18}O + ^{30}Si reaction

As predicted by the statistical code, the three particle evaporation channels leading to residues with A = 45 are dominant at 55 MeV of beam energy, whereas, in the bombardment by the more energetic projectiles of 65 MeV mainly four particles are emitted. Even though, at 65 MeV bombarding energy we did observe a relative increase of the yield of high spin states in ^{45}Sc as illustrated in Fig. 2. Moreover, several transitions with high intensity, not known earlier, were identified as belonging to the mass A = 45, and most probably depopulating high-spin states.

2.2 Multiple γ-coincidences measurements

The promising results of the pilot measurement encouraged us to run a multiple γ-coincidence experiment with the same beam/target combination but at an intermediate beam energy of 60 MeV. Two consecutive runs were

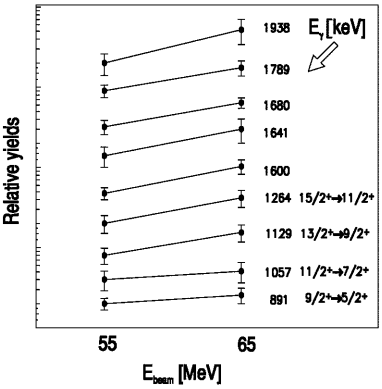

Fig. 2. Relative yields of the known high spin states in ^{45}Sc and several new levels identified as belonging to the A = 45 mass, measured for two beam energies 55 MeV and 65 MeV

performed, one with a thick target of 7 mg/cm^2 ^{30}SiO$_2$ and the other with a thin one of 300 mg/cm^2 ^{30}Si. In this experiment we made use of the GASP multidetector array [21] to detect γ-rays. The GASP array at that time consisted of 36 Compton suppressed HPGe detectors and of 80 BGO scintillators, operating as a multiplicity filter and a sum spectrometer. The energy gain of the amplifiers was set as to measure γ-transitions up to 4 MeV, which were expected to de-excite high spin states in the nuclei of interest. Events were collected on tape when at least two germanium detectors and two BGO elements fired in coincidence. Gamma-ray energy and time information from the Ge detectors was recorded as well as the γ-multiplicity and the total energy registered by the BGO ball. To reduce random coincidences, in the off-line sorts only events containing prompt (with respect to the BGO ball) Ge signals were accepted.

In addition, during the thin target measurement the GASP was used in coupling to the RMS as described in [22]. The RMS signals: X, Y and TOF were treated as additional parameters in the acquisition system.

2.2.1 Thick target measurement

From the thick target γ-γ coincidence total projection spectra we have determined the relative population of the different reaction channels taking into account all transitions leading to the ground states. In Fig. 3 we report the relative intensity of each evaporation channel normalized to the total fusion cross section. The strongest channels α2n and p2n being respectively about 40% and 30% of the compound nucleus decay lead to ^{42}Ca and ^{45}Sc final nuclei. The ^{43}Ca and ^{45}Ti nuclei were produced after αn and 3n emission with a cross section of about 10% each. The remaining 10% of the total cross section was distributed between weakly populated residua as: ^{41,44,45}Ca, ^{44}Sc, ^{46}Ti, ^{41}K and ^{38}Ar. The statistical code estimations are also displayed in Fig. 3 and generally agree with the measured distribution.

The data of this thick target experiment were not used for the extraction of the level schemes at high spins of the nuclei of interest. In fact, due to the high recoil velocity (v/c = 3%) and the consequent shift and broadening of γ-rays caused by the Doppler effect, the resulted spectra were too complicated for a meaningful analysis.

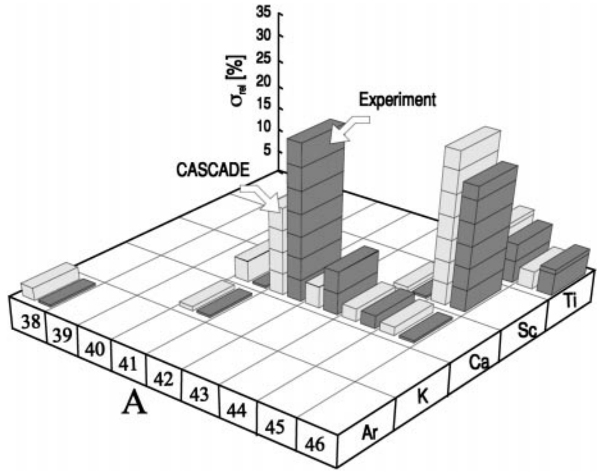

Fig. 3. Distribution of the measured and calculated with the CASCADE code total fusion cross section for the reaction induced by 65 MeV ^{18}O ions on a thick ^{30}Si target

The high spin properties of the ^{45}Sc, ^{45}Ti and ^{43}Ca nuclei have been extracted from the analysis of the thin target data.

2.2.2 Thin target measurement

Double and triple γ-coincidence data from the thin target experiment were used to extend the level schemes at high spin of the nuclei: ^{45}Sc, ^{45}Ti and ^{43}Ca.

The high-energy γ-lines attributed to A = 45 nuclei in the pilot RMS experiment could then be placed in the level schemes of ^{45}Sc and ^{45}Ti. Additionally, several new transitions were identified and assigned to ^{45}Sc or to ^{45}Ti, which were also seen in γ-recoil spectrum measured in coincidence with mass A = 45. The γ-recoil coincidence was useful for a better determination of the energy of γ-ray transitions. In fact, the high energy γ-lines seen in coincidence with fast moving recoils (v/c = 3%), due to the small opening angle of RMS, revealed significant reduction of the excessive Doppler broadening. An example of almost 30% reduction of the FWHM of the 1725 keV line originating from ^{45}Sc, obtained when γ-recoil coincidences were required, is illustrated in Fig. 4. Unfortunately, a low RMS efficiency of the order of 1% in this experiment made the use of higher fold γ-recoil coincidences impossible.

2.2.3 The DCO analysis

The studies of the angular distribution of γ-rays were performed in order to determine spins of the identified levels.

We applied the DCO method as described in [23]. The DCO ratio factor was calculated as: $R_{DCO} = I(\gamma_1, \theta_1; \gamma_2, \theta_2)/I(\gamma_1, \theta_2; \gamma_2, \theta_1)$, where $I(\gamma_1, \theta_1; \gamma_2, \theta_2)$

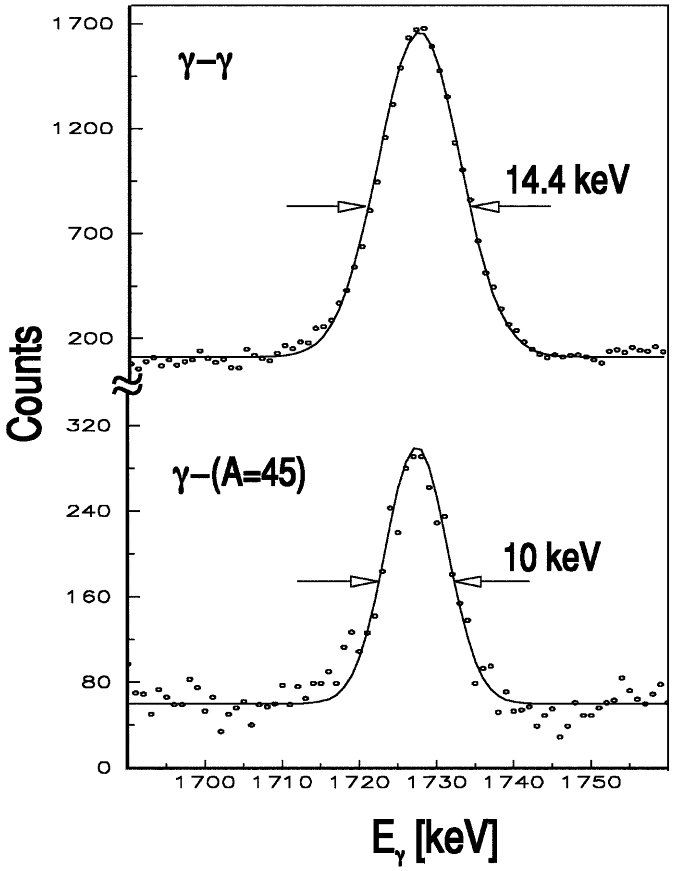

Fig. 4. Example of the FWHM reduction for a γ-line obtained by the γ-recoil coincidences when using RMS

is the intensity of the transition γ_1 measured at the angle θ_1 with respect to the beam direction, in coincidence with the transition γ_2 detected at the angle θ_2. According to the GASP geometry, we compared the two peak areas in the summed spectra of the most forward and the most backward detectors placed at $\theta_1 = 36°$ or 144° with those seen at $\theta_2 = 90°$. The obtained RDCO ratios were compared with the values calculated on the basis of the approach described by Krane [24].

Additionally, the analysis of the angular distribution of γ-rays in coincidence with the recoils measured by the RMS, confirmed the deduced multipolarities of the most intense transitions.

2.2.4 Lifetime measurement

In order to determine the lifetimes of the excited states in ^{45}Sc and ^{45}Ti by means of the DSAM, we applied the ^{12}C(^{35}Cl,2p)^{45}Sc and ^{12}C(^{35}Cl,pn)^{45}Ti reverse kinematics fusion evaporation reactions. The thickness of 15 mg/cm^2 for the ^{12}C target was chosen to stop the recoils. The initial ^{35}Cl beam energy of 75 MeV was slightly above the barrier in order to open mainly two particle evaporation channels. Afterwards, the projectile energy was raised to 95 MeV and then 120 MeV. In this stepwise way, the different regions of spins and excitation energies in ^{45}Sc and ^{45}Ti were selected which allowed for the side-feeding evaluation. This is illustrated in Figure 5 where γ-ray spectra showing mainly transitions from ^{45}Sc are compared for the highest and lowest beam energy. The increase of the relative intensities of the γ-transitions emitted from the high spin states for the more energetic projectiles is clearly observed.

The γ-rays were detected in the GASP array which was of its full configuration of 40 germanium detectors. The trigger conditions for the acquisition system were similar as those in the previous experiment. We analysed γ-rays spectra taken at the forward and the backward angles in coincidence with the unshifted transitions de-exciting the low lying levels from ^{45}Sc and ^{45}Ti. The experimental line-shapes were compared with the simulations performed as prescribed in [25]. Examples of the best fits obtained from the line shape simulations for some selected transitions in ^{45}Sc and ^{45}Ti are shown in Fig. 6.

In the line shape calculations we took into account the decay of the known states lying above each level. An instantaneous side-feeding was also assumed. Comparison of the calculations with the line shapes obtained for the beam energy of 75 MeV allowed to minimize the effect of the effective lifetime accumulation significant in the case of the low lying levels fed by γ-cascades. On the other hand, the use of the more energetic beams allowed to extract the lifetimes of the highly excited states.

The side-feeding influencing the line-shapes was estimated on the basis of the γ-spectra measured at 90°. Ex-

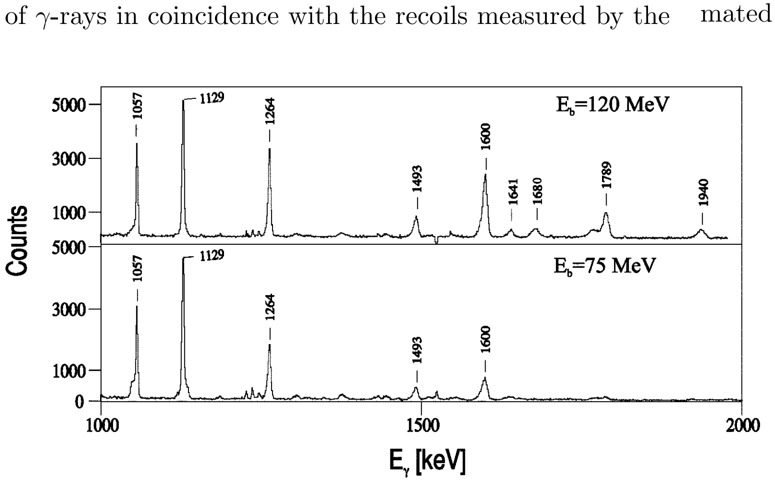

Fig. 5. Gamma spectra measured for the 75, 120 MeV ^{35}Cl + ^{12}C reaction. The increase of the population of high spin states above $J^\pi = 19/2^+$ level in ^{45}Sc is seen (see also the level scheme in Fig. 8)

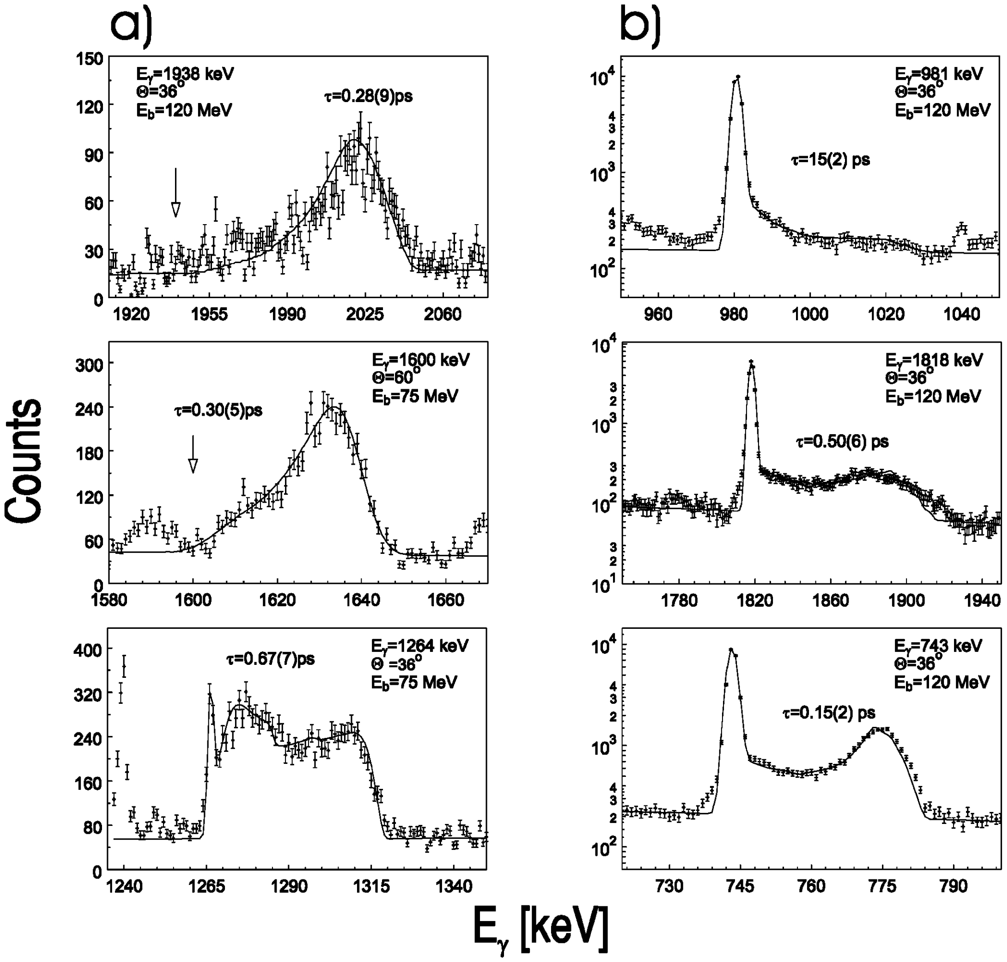

Fig. 6. Examples of the DSAM line-shape evaluations obtained for selected transitions in ^{45}Sc **a** ^{45}Ti **b**

ample of the intensity distribution of the side-feeding determined for the positive parity band in ^{45}Sc at the beam energy of 120 MeV is shown in Fig. 7.

The line-shape evaluation was done assuming that the directions of the recoils did not alter in the target/stopper material. This condition is reasonable for such a light stopper as ^{12}C where the total stopping power is determined entirely by its electronic component in the whole energy range. The stopping power necessary for the stopping process simulation was taken from the tables of Ziegler [26]. Although, to obtain the best fit to the experimental data the dE/dx values for the recoil energies less than 0.2 MeV/A were decreased by 20%.

In the simulation, the loss of the energy of the projectile penetrating the thick ^{12}C target was taken into account. The final line shapes were obtained by summing spectra calculated for various projectile energies (ranging from the energy provided by the accelerator to the barrier energy) and weighted by the relative reaction cross section provided by the CASCADE code. The applied method allowed to establish lifetimes ranging from a few ps to 0.1 ps with the accuracy of the order of 10–20% of the measured values.

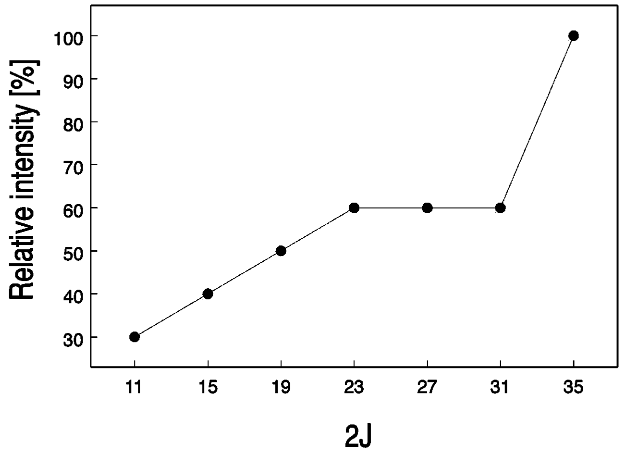

Fig. 7. Side-feeding distribution in the 120 MeV ^{35}Cl + ^{12}C reaction determined for the positive parity band A in ^{45}Sc (cf. the level scheme in Fig. 8)

3 Results

3.1 The nucleus ^{45}Sc

The level scheme of the ^{45}Sc nucleus, deduced from the present experiment is shown in Fig. 8. The energies of some γ-rays are corrected with respect to the previously

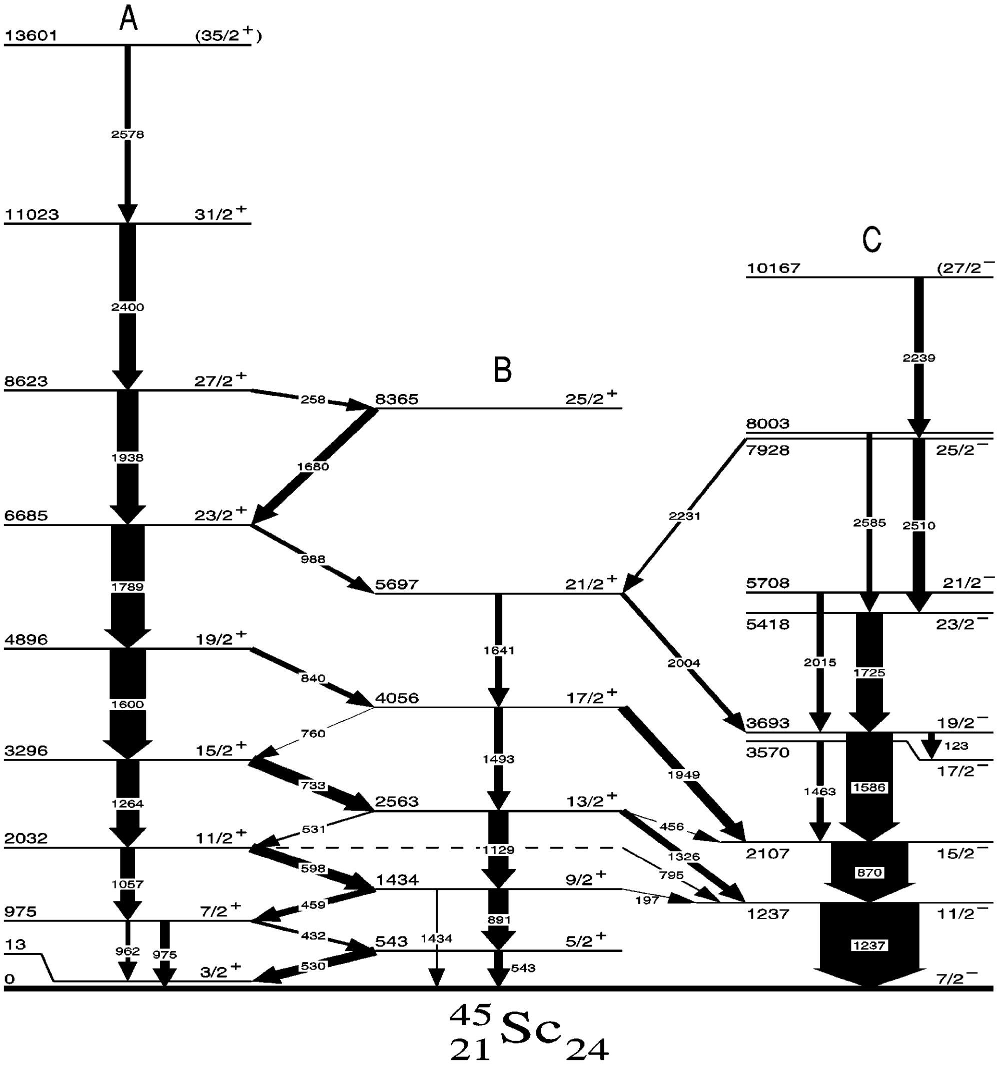

Fig. 8. Level scheme of ^{45}Sc obtained in course of the present work with γ-ray intensities from the ^{18}O + ^{30}Si reaction

reported data [16] due to now better energy calibration obtained in the lifetime measurement experiment. Also the γ-transition of 3070 keV proposed in the [16] as feeding the highest $35/2^+$ level is not seen in this experiment, therefore it is not included in the presented here level scheme.

The states known prior to our work up to 3296 keV, $15/2^+$, for positive parity and 5418 keV, $23/2^-$, for negative parity have been confirmed and both positive and negative parity structures have been significantly extended towards higher spins and excitation energies.

In particular, we have identified a rotational-like cascade composed of high energy E2 transitions: 1600 keV, 1789 keV, 1938 keV and 2400 keV feeding the 3296 keV level (see the γ-ray spectrum in Fig. 9a).

Consequently the $19/2^+$, $23/2^+$, $27/2^+$ and $31/2^+$ states at energies: 4896 keV, 6685 keV, 8623 keV and 11023 keV, respectively, have been added to the band marked A in the level scheme in Fig. 8.

The 13601 keV state is most likely the highest member of the band with a tentative J^π assignment of $35/2^+$. The 2578 keV transition depopulating this level is too weak to determine its multipolarity by means of the DCO analysis.

The structure marked B in the ^{45}Sc level scheme has also been extended by two new levels 4056 keV, $J^\pi = 17/2^+$ and 5697 keV, $J^\pi = 21/2^+$ decaying via E2 transitions 1493 keV and 1641 keV, respectively. In addition, the series of M1 γ-rays: 760 keV, 840 keV, 988 keV, 1680 keV and 258 keV connecting the two bands A and B has been found. The obtained DSAM results point out that the lifetimes of the positive parity states gradually decrease with increasing spin, reaching the observation limit of 0.1 ps for the $31/2^+$ state.

The negative parity structure in ^{45}Sc has been extended by four new levels at excitation energies of: 5708 keV, 7928 keV, 8003 keV and 10167 keV. They decay by emitting γ-rays: 2015 keV, 2510 keV, 2585 keV and 2239 keV, respectively, (see Fig. 9b). For the two levels at 5708 keV and 7928 keV the DCO ratio analysis has led to a spin assignment $21/2^-$ and $25/2^-$, respectively. The $J^\pi = 27/2^-$ assignment proposed for the highest 10167 keV level is based on the comparison with the shell model calculations (see Discussion and Fig. 14 therein).

Four new transitions: 456 keV, 1949 keV, 2004 keV and 2231 keV connecting several opposite parity states have been also found in this experiment.

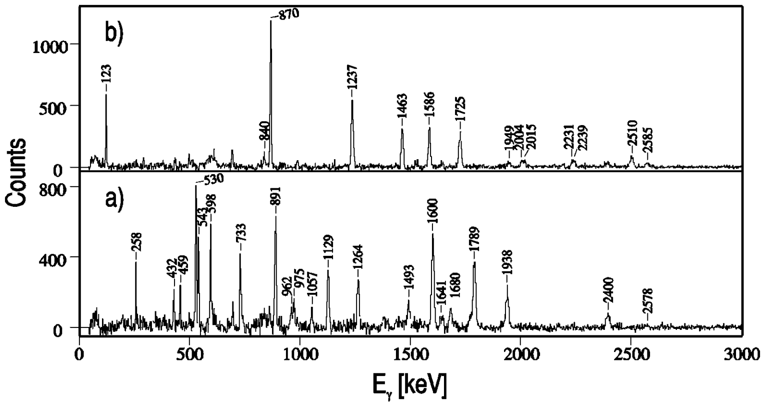

Fig. 9. Triple-γ coincidence spectra obtained by double gating on the known transitions depopulating the positive **a** negative **b** levels in ^{45}Sc

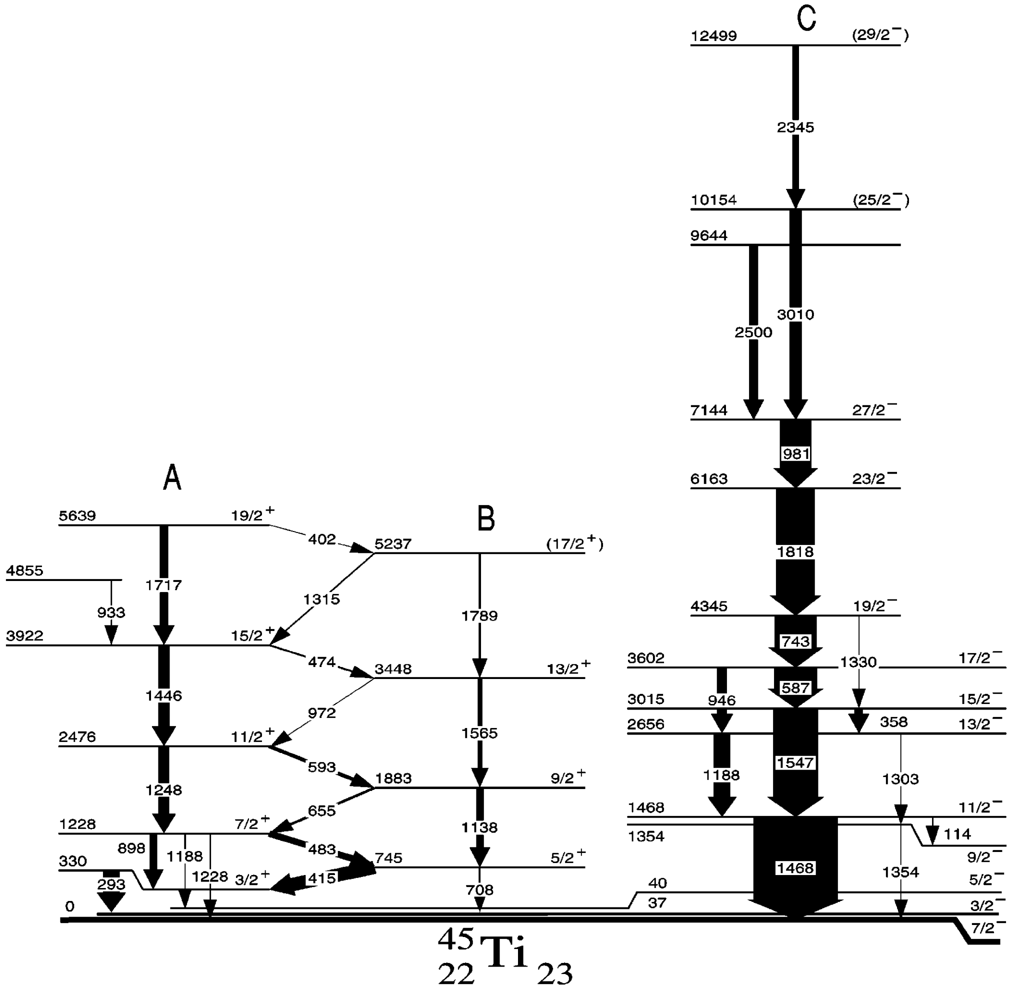

Fig. 10. Level scheme of ^{45}Ti

Most of the newly observed highly excited negative parity states are short-lived with τ below 0.1 ps.

In Tables 1a and 1b energies and relative intensities of the γ-rays belonging to the ^{45}Sc nucleus are summarised. The experimental DCO ratios are also given as well as those expected for the assumed spins. It is easy to distinguish between E2 transitions which have $R_{DCO} \approx 1$ and M1 transitions with R_{DCO} significantly grater than unity.

Our DSAM studies have provided lifetimes for most of the observed levels as displayed in the tables. For the few low-spin states where lifetimes were already known from previous experiments [27], our results are in rather good agreement.

3.2 The nucleus ^{45}Ti

As mentioned in Sect. 2.2.1, the ^{45}Ti nucleus was populated about three times weaker than ^{45}Sc in the reaction used in this work. However, its structure has been also significantly extended (cf. [27]), as it can be seen from the level scheme in Fig. 10. The results are summarised in Ta-

Table 1. a. Collected information on the properties and the decay of the positive parity levels observed in ^{45}Sc

E_i [keV]	E_f [keV]	I_i^π	I_f^π	E_γ [keV]	Int_γ	B.R %	R_{DCO}		τ [ps]	
							experiment	theory	measu-rement	literature ref. [27]
543		5/2$^+$							–	7.9 *9*
	0		7/2$^-$	543	83	27	–	–		
	13		3/2$^+$	530	183	73	–	–		
975		7/2$^+$							–	3.66 *33*
	0		7/2$^-$	975	101	55	–	–		
	13		3/2$^+$	962	43	23	–	–		
	543		5/2$^+$	432	40	22	–	–		
1434		9/2$^+$							–	5.2 *3*
	0		7/2$^-$	1434	20	6	–	–		
	543		5/2$^+$	891	207	64	–	–		
	975		7/2$^+$	459	85	26	–	–		
	1237		11/2$^-$	197	9	4	–	–		
2032		11/2$^+$							1.4 *2*	1.02 *30*
	975		7/2$^+$	1057	146	49	–	–		
	1237		11/2$^-$	795	18	6	–	–		
	1434		9/2$^+$	598	136	45	1.72 *15*[a]	2.0		
2563		13/2$^+$							1.5 *4*	2.0 *9*
	1237		11/2$^-$	1326	87	22	–	–		
	1434		9/2$^+$	1129	204	51	0.94 *4*[a]	1		
	2032		11/2$^+$	531	68	6	–	–		
	2107		15/2$^+$	456	85	21	–	–		
3296		15/2$^+$							0.67 *7*	–
	2032		11/2$^+$	1264	230	59	1.06 *15*[b]	1		
	2563		13/2$^+$	733	161	41	2.02 *12*[a]	1.87		
4056		17/2$^+$							0.40 *9*	–
	2107		15/2$^-$	1949	114	54	1.49 *16*[c]	1.83		
	2563		13/2$^+$	1493	89	42	1.11 *20*[a]	1		
	3296		15/2$^+$	760	10	4	–			
4896		19/2$^+$							0.30 *5*	–
	3296		15/2$^+$	1600	364	84	1.15 *10*[d]	1		
	4056		17/2$^+$	840	71	16	–	–		
5697		21/2$^+$							0.4 *2*	–
	3693		19/2$^-$	2004	56	44	1.57 *10*[c]	1.78		
	4056		17/2$^+$	1641	72	56	0.88 *11*[d]	1		
6685		23/2$^+$							0.25 *5*	–
	4896		19/2$^+$	1789	329	86	0.96 *9*[e]	1		
	5697		21/2$^+$	988	52	14	–	–		
8365		25/2$^+$							<0.1	–
	6685		23/2$^+$	1680	108	100	2.22 *46*[f]	1.75		
8623		27/2$^+$							0.28 *9*	–
	6685		23/2$^+$	1938	219	82	1.04 *14*[f]	1		
	8365		25/2$^+$	258	48	18	1.69 *42*[f]	1.74		
11023		31/2$^+$							<0.1	–
	8623		27/2$^+$	2400	164	100	1.03 *20*[g]	1		
13601		(35/2$^+$)							<0.1	–
	11023		31/2$^+$	2578	53	100	–	–		

The experimental R_{DCO} ratios were evaluated with the following gate settings: [a] −891 keV, [b] −1057 keV, [c] −870 keV, [d] −1264 keV, [e] −1600 keV, [f] −1789 keV, [g] −1938 keV

Table 1. b. Collected information on the properties and the decay of the negative parity levels observed in ^{45}Sc

E_i [keV]	E_f [keV]	I_i^π	I_f^π	E_γ [keV]	Int_γ	B.R %	R_{DCO} experiment	R_{DCO} theory	τ [ps] measurement	τ [ps] literature ref. [27]
1237		$11/2^-$							–	2.60 *14*
	0		$7/2^-$	1237	1000	100	–	–		
2107		$15/2^-$							–	>2
	1237		$11/2^-$	870	783	100	0.93 *2*	1		
3570		$17/2^-$							<0.1	–
	2107		$15/2^-$	1463	75	100	2.24 15	1.83		
3693		$19/2^-$							2.0 *2*	–
	2107		$15/2^-$	1586	472	87	0.96 5	1		
	3570		$17/2^-$	123	68	13	1.50 15	1.81		
5418		$23/2^-$							1.9 *2*	–
	3693		$19/2^-$	1725	269	100	0.99 7	1		
5708		$21/2^-$							–	–
	3693		$19/2^-$	2015	78	100	1.57 20	1.78		
7928		$25/2^-$							<0.1	–
	5418		$23/2^-$	2510	112	76	1.94 27	1.75		
	5697		$21/2^+$	2231	36	23	–	–		
	8003		–						<0.1	–
	5418		$23/2^-$	2585	53	100	–	–		
10167		$(27/2^-)$							<0.1	–
	7928		$25/2^-$	2239	92	100	–	–		

The experimental R_{DCO} ratios were obtained for the 1237 keV gate setting

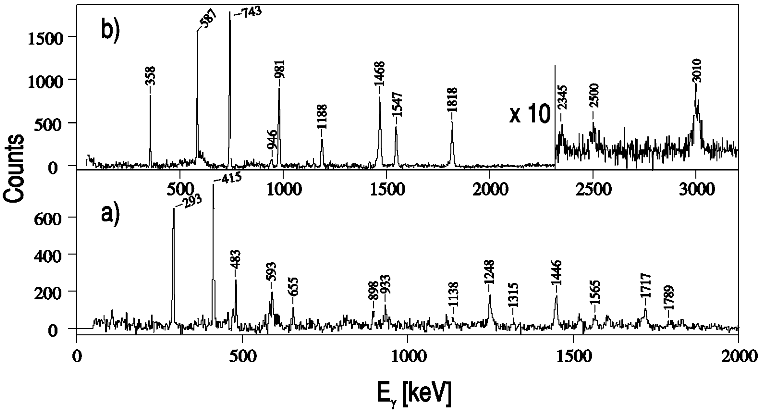

Fig. 11. Spectra of γ-rays depopulating the positive **a** negative **b** levels in ^{45}Ti doubly gated on all known γ-transitions

bles 2a and 2b, respectively, for the positive and negative parity states.

Particularly, the rotational-like structures labelled A and B in the level scheme of Fig. 10 have been extended to higher spins by identification of new states: 3922 keV, $J^\pi = 15/2^+$, 5639 keV, $J^\pi = 19/2^+$ and 3448 keV, $J^\pi = 13/2^+$, 5237 keV, $J^\pi = (17/2^+)$ decaying through the series of E2 γ-ray transitions: 1446 keV, 1717 keV and 1565 keV, 1789 keV (see Fig. 11a).

In addition, the interband M1 transitions: 972 keV, 474 keV, 1315 keV, and 402 keV which connect the levels belonging to the bands A and B have been observed.

In the coincidence spectra shown in Fig. 11a, the 933 keV line feeding the 3922 keV level with $J^\pi = 15/2^+$ is also clearly seen.

Moreover, in our experiment the 1463 keV line proposed in [1] as a transition between the $15/2^+$ and $11/2^+$ states has not been confirmed.

The spin assignment of the positive parity states in ^{45}Ti is based mainly on the observed decay pattern. Although the DCO ratios were measured, the R_{DCO} factors are similar for the transitions between states differing by $\Delta I = 1$ and $\Delta I = 2$. This is due to the significant admixture of E2 component in the radiation emitted in the $\Delta I = 1$ case. The mixing ratios which emerge from the comparison between the experimental data and the calculated DCO ratios are in accord with the experimental values known from the literature [27]: $\delta = +0.4$ for the 415 keV transition, $\delta = +0.3$ for both 483 keV and 655 keV lines, $\delta = +0.1$ for 593 keV transition.

As in the ^{45}Sc case, the measured lifetimes for the states below the $11/2^+$ state are in good agreement with the values known from the previous studies [27], as it is shown in Table 2a. New information is obtained on the lifetimes for the high spin states.

Table 2. a. Collected information on the properties and the decay of the positive parity levels observed in ^{45}Ti

E_i [keV]	E_f [keV]	I_i^π	I_f^π	E_γ [keV]	Int_γ	B.R %	R_{DCO}		τ [ps]	
							experiment	theory	measurement	literature ref. [27]
330		$3/2^+$							–	585 *19*
	37		$3/2^-$	293	195	100	–	–		
744		$5/2^+$							–	15.1 *2*
	37		$3/2^-$	708	13	6	–	–		
	330		$3/2^+$	415	183	94	0.82 *7*	0.93		
1228		$7/2^+$							–	4.0 *8*
	0		$7/2^-$	1228	13	6	–	–		
	40		$5/2^-$	1188	11	6	–	–		
	330		$3/2^+$	898	89	45	0.74 *10*	0.73		
	745		$5/2^+$	483	86	43	0.80 *11*	1.0		
1883		$9/2^+$							1.0 *1*	1.0 *2*
	745		$5/2^+$	1138	90	73	0.64 *11*	0.75		
	1228		$7/2^+$	655	33	27	0.96 *20*	0.85		
2476		$11/2^+$							0.5 *1*	0.65 *13*
	1228		$7/2^+$	1248	131	73	0.75 *10*	0.79		
	1883		$9/2^+$	593	48	27	0.85 *15*	1.25		
3448		$13/2^+$							0.26 *3*	–
	1883		$9/2^+$	1565	52	80	0.79 *16*	0.77		
	2476		$11/2^+$	972	13	20	–	–		
3922		$15/2^+$							0.45 *3*	–
	2476		$11/2^+$	1446	135	87	0.66 *10*	0.82		
	3448		$13/2^+$	474	20	13	–	–		
4855									0.50 *7*	–
	3922		$15/2^+$	933	13	100	–	–		
5237		$(17/2^+)$							0.10 *9*	–
	3448		$13/2^+$	1789	30	63	–	–		
	3922		$15/2^+$	1315	17	37	–	–		
5639		$19/2^+$							0.27 *8*	–
	4855		$15/2^+$	1717	101	93	0.68 *11*	0.83		
	5237		$(17/2^+)$	402	8	7	–	–		

The experimental R_{DCO} ratios were obtained for the 293 keV gate setting

In the present work, three new negative parity states above the known $J^\pi = 27/2^-$ state at 7144 keV have been found. These states with energies: 9644 keV, 10154 keV and 12499 keV decay to the negative parity states via 2500 keV, 3010 keV, 2345 keV γ-radiation, respectively, as is seen in the structure C in the ^{45}Ti level scheme (see also Fig. 11b).

Comparing the relative intensities of the sequentially emitted transitions: 1818 keV and 743 keV, we conclude that their previous ordering [4] should be inverted: the 743 keV γ-ray depopulates the 4345 keV, $19/2^-$, state, whereas the 1818 keV transition de-excites the 6163 keV, $23/2^-$, state. This conclusion is further confirmed by the observation of the crossover transition of 1330 keV.

The obtained DCO ratios confirm the previous spin assignments of the known levels lying above the $11/2^-$ state. Despite poor statistics, the DCO ratio indicates a strong anisotropy for the 3010 keV line. Such a behaviour points out that the spin of the 10154 keV level may be either $25/2^-$ or $29/2^-$. The comparison of the observed level structure with the shell model calculations (see Fig. 14 in the Discussion) suggests that the two highest excited states i.e. 10154 keV and 12499 keV should have spins $J^\pi = 25/2^-$ and $J^\pi = 29/2^-$, respectively.

The lifetimes of the states above 1468 keV, $J^\pi = 11/2^-$ have been measured for the first time in the present experiment. A characteristic feature is the relatively large τ value for the $J^\pi = 27/2^-$, 7144 keV state, which is one order of magnitude larger than the typical value for the rest of the $\pi = -$ levels. Therefore, the line-shapes of the transitions emitted in the decay of the short-living states lying below contain both the stopped and the shifted components (see Fig. 6b in Sect. 2.2.4) related to the feeding from above and to the direct side-feeding.

3.3 The nucleus ^{43}Ca

The level scheme of ^{43}Ca derived from our measurements is shown in Fig. 12. and fully agrees with previous findings [5]. The only new γ-transition found is the weak 993 keV line connecting the 3944 keV, $15/2^+$ and 2951, keV $11/2^+$ states. As in ^{45}Sc and ^{45}Ti, this nucleus also presents a rotational like sequence of positive parity states. However,

Table 2. b. Collected information on the properties and the decay of the negative parity levels observed in ^{45}Ti

E_i [keV]	E_f [keV]	I_i^π	I_f^π	E_γ [keV]	Int$_\gamma$	B.R %	R$_{DCO}$ experiment	R$_{DCO}$ theory	τ [ps] measurement	τ [ps] literature ref. [27]
1354		$9/2^-$							–	0.15 *1*
	0		$7/2^-$	1354	11	100	–	–		
1468		$11/2^-$							–	0.69 *10*
	0		$7/2^-$	1468	1000	99	–	–		
	1354		$9/2^-$	114	10	1	–	–		
2656		$13/2^-$							<0.25	–
	1354		$9/2^-$	1302	11	5	–	–		
	1468		$11/2^-$	1188	198	95	1.96 *14*^{a}	1.92		
3015		$15/2^-$							0.8 *2*	–
	1468		$11/2^-$	1547	531	84	1.01 *10*^{a}	1		
	2656		$13/2^-$	358	100	16	1.75 *30*^{a}	1.79		
3602		$17/2^-$							1.3 *1*	–
	2656		$13/2^-$	946	115	18	1.02 *15*^{b}	1		
	1468		$15/2^-$	587	509	82	1.78 *11*^{b}	1.83		
4345		$19/2^-$							0.15 *2*	–
	3015		$15/2^-$	1330	9	2	–	–		
	743		$17/2^-$	743	499	98	1.60 *19*^{b}	1.80		
6163		$23/2^-$							0.50 *6*	–
	4345		$19/2^-$	1818	459	100	0.98 *17*^{b}	1		
7144		$27/2^-$							15 *2*	–
	6163		$23/2^-$	981	378	100	0.85 *13*^{b}	1		
9644									<0.1	–
	7144		$27/2^-$	2500	100	100	–	–		
10154		$(25/2^-)$							<0.1	–
	7144		$27/2^-$	3010	141	100	>1^{c}	1.7		
12499		$(29/2^-)$							<0.1	–
	10154		$(25/2^-)$	2345	78	100	–	–		

The experimental R$_{DCO}$ ratios were obtained for the gate settings: ^{a} −1468 keV, ^{b} −1547 keV, ^{c} −981 keV

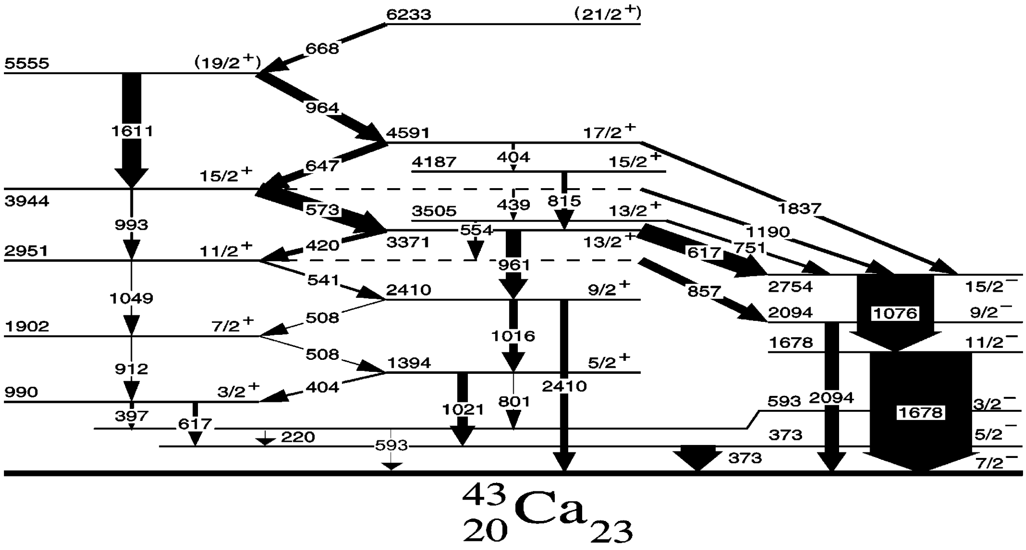

Fig. 12. Level scheme of ^{43}Ca

Table 3. Collected information on the properties and the decay of the levels observed in ^{43}Ca

E_i [keV]	E_f [keV]	I_i^π	I_f^π	E_γ [keV]	Int_γ
373		$5/2^-$			
	0		$7/2^-$	373	339
593		$3/2^-$			
	0		$7/2^-$	593	20
	373		$5/2^-$	220	10
990		$3/2^+$			
	593		$3/2^-$	397	36
1394		$5/2^+$			
	373		$7/2^+$	1021	101
	593		$3/2^-$	801	3
	990		$3/2^+$	404	26
1678		$11/2^-$			
	0		$7/2^-$	1678	1000
1902		$7/2^+$			
	990		$3/2^+$	912	11
	1394		$5/2^+$	508	12
2094		$7/2^-$			
	0		$7/2^-$	2094	139
2410		$9/2^+$			
	0		$7/2^-$	2410	75
	1394		$5/2^+$	1016	82
	1902		$7/2^+$	508	12
2754		$15/2^-$			
	1678		$11/2^-$	1076	754
2951		$11/2^+$			
	1902		$7/2^+$	1049	10
	2094		$9/2^-$	857	105
	2410		$9/2^+$	541	29
3371		$13/2^+$			
	2410		$9/2^+$	961	140
	2754		$15/2^-$	617	49
	2951		$11/2^+$	420	65
3505		$13/2^+$			
	2754		$15/2^-$	751	36
	2951		$11/2^+$	554	19
3944		$15/2^+$			
	2754		$15/2^-$	1190	45
	2951		$11/2^+$	993	19
	3371		$13/2^+$	573	196
	3505		$13/2^+$	439	20
4187		$15/2^+$			
	3371		$13/2^+$	815	46
4591		$17/2^+$			
	2754		$15/2^-$	1837	45
	3944		$15/2^+$	647	96
	4187		$15/2^+$	404	29
5555		$(19/2^+)$			
	3944		$15/2^+$	1611	186
	4591		$17/2^+$	964	123
6233		$(21/2^+)$			
	5555		$(19/2^+)$	668	54

the comparison of the relative intensities of the transitions points out that the $\pi = +$ levels decay mainly to the negative parity states. For ^{43}Ca we have not measured the lifetimes for the excited states as in the reversed reaction used in the DSAM measurement ^{43}Ca was not populated.

The information on the γ-decay of excited levels in ^{43}Ca is summarised in Table 3.

4 Discussion

All three studied odd-A nuclei i.e. ^{43}Ca, ^{45}Sc and ^{45}Ti exhibit a nice example of a coexistence of spherical and deformed structures. The spherical structure which is viewed by the negative parity states is mainly due to the excitations within the fp shell while the positive parity states involve sd-fp cross-shell excitations and thus are much more collective in the number of incorporated quasi-particles both protons and neutrons and the respective holes. This collectivity shows-up in the straight lines when excitation energy is plotted versus square of the angular momentum $J(J+1)$ as is displayed in Fig. 13.

The deformed prolate structure having positive deformation parameter β was supposed already some time ago [3], where the sign of the intrinsic quadrupole moment was determined from the sign of the mixing ratio and the magnetic moment, of course, under assumption of the rotational band.

In our recent publication [18], we have demonstrated that the total routhian surface calculation by the Woods-Saxon-Strutinski method including pairing [28] do show that the positive-parity structure in ^{45}Sc is deformed, with $\beta \approx 0.2$ which is to be compared with the experimental deformation parameter $\beta_{\mathrm{exp}} = 0.24$ – an averaged value for the whole band, obtained from the data in Table 4. For ^{45}Ti that averaged value of the deformation parameter is larger, $\beta_{\mathrm{exp}} = 0.33$, suggesting even bigger deformation in this nucleus. This may be the cause that the outerband E1 transitions between the positive and the negative structures are not observed for ^{45}Ti while in ^{45}Sc they occur. In the ^{43}Ca case where the rotational features of the $\pi = +$ levels are not so evident such E1 transitions dominate.

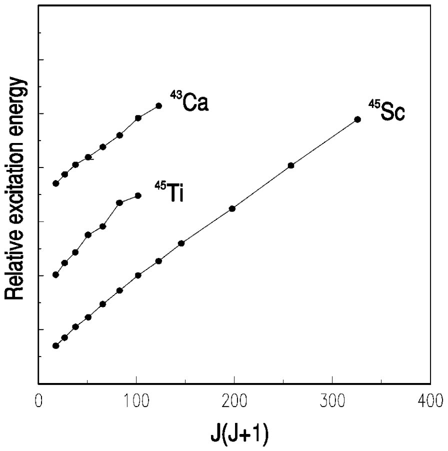

Fig. 13. Relative excitation energy versus $J(J+1)$ for the positive parity states in ^{45}Sc,^{45}Ti and ^{43}Ca

Table 4. Experimental B(E2) transition rates, quadrupole moments and deformation parameters deduced for the positive parity levels in ^{45}Sc (a) and ^{45}Ti (b)

E_γ [keV]	$I_i^\pi \rightarrow I_f^\pi$	$B(E2)_{exp}$ 1) [e^2fm^4]	Q_0 2) [barn]	β 3)
(a)		^{45}Sc		
962	$7/2^+ \rightarrow 3/2^+$	62 *12*	0.66 *6*	0.23 *2*
891	$9/2^+ \rightarrow 5/2^+$	179 *28*	0.92 *7*	0.32 *2*
1057	$11/2^+ \rightarrow 7/2^+$	216 *53*	0.92 *11*	0.32 *4*
1129	$13/2^+ \rightarrow 9/2^+$	151 *55*	0.74 *14*	0.25 *5*
1264	$15/2^+ \rightarrow 11/2^+$	223 *45*	0.87 *9*	0.30 *3*
1493	$17/2^+ \rightarrow 13/2^+$	115 *55*	0.6 *1*	0.21 *3*
1600	$19/2^+ \rightarrow 15/2^+$	218 *80*	0.83 *11*	0.29 *4*
1641	$21/2^+ \rightarrow 17/2^+$	96 *58*	0.55 *16*	0.19 *6*
1789	$23/2^+ \rightarrow 19/2^+$	153 *45*	0.68 *10*	0.23*4*
1938	$27/2^+ \rightarrow 23/2^+$	87 *37*	0.51 *11*	0.18 *4*
2400	$31/2^+ \rightarrow 27/2^+$	>102	>0.55	>0.19
2578	$(35/2^+) \rightarrow 31/2^+$	>172	>0.45	>0.16
(b)		^{45}Ti		
1138	$9/2^- \rightarrow 5/2^-$	312 *62*	1.21 *12*	0.40 *4*
1248	$11/2^+ \rightarrow 7/2^+$	393 *118*	1.24 *19*	0.41 *6*
1565	$13/2^+ \rightarrow 9/2^+$	267 *58*	0.98 *11*	0.32 *3*
1446	$15/2^+ \rightarrow 11/2^+$	250 *42*	0.92 *7*	0.30 *3*
1789	$(17/2^+) \rightarrow 13/2^+$	280 *280*	0.9 *5*	0.3 *2*
1717	$19/2^+ \rightarrow 15/2^+$	188 *75*	0.77 *15*	0.26 *5*

1) The reduced transition probability was calculated according to the formula

$$B(E2) = 8.16PE^5\tau\,[e^2fm^2]$$

2) The intrinsic quadrupole moment is extracted from the expression

$$B(E2;\, I_1 \rightarrow I_2) = 5/16\,\pi e^2 Q_0^2 \langle I_1 2K0|I_2K\rangle^2$$

3) The deformation parameter is obtained from the relation

$$Q_0 \simeq (3/\sqrt{5\pi})ZR_0^2\beta(1+0.36\beta)$$

Table 5. Experimental B(M1) transition reduced for the positive parity levels in ^{45}Sc (a) and ^{45}Ti (b)

E_γ [keV]	$I_i^\pi \rightarrow I_f^\pi$	$B(M1)_{exp}$ 1) [μ_N^2]
(a)	^{45}Sc	
530	$5/2^+ \rightarrow 3/2^+$	0.027 *6*
432	$7/2^- \rightarrow 5/2^+$	0.039 *8*
459	$9/2^+ \rightarrow 7/2^+$	0.023 *4*
598	$11/2^+ \rightarrow 9/2^+$	0.08 *2*
531	$13/2^+ \rightarrow 11/2^+$	0.015 *1*
733	$15/2^+ \rightarrow 13/2^+$	0.08 *2*
760	$17/2^+ \rightarrow 15/2^+$	0.013 *3*
840	$19/2^+ \rightarrow 17/2^+$	0.050 *8*
988	$23/2^+ \rightarrow 21/2^+$	0.033 *7*
1680	$25/2^+ \rightarrow 23/2^+$	>0.12
258	$27/2^+ \rightarrow 25/2^+$	2.1 *9*
(b)	^{45}Ti	
415	$5/2^+ \rightarrow 3/2^+$	0.042 *5*
483	$7/2^+ \rightarrow 3/2^+$	0.049 *5*
655	$9/2^+ \rightarrow 7/2^+$	0.050 *10*
593	$11/2^+ \rightarrow 9/2^+$	0.14 *4*
972	$13/2^+ \rightarrow 11/2^+$	0.047 *10*
474	$15/2^+ \rightarrow 13/2^+$	0.15 *3*
1315	$17/2^+ \rightarrow 15/2^+$	0.09 *9*
402	$19/2^+ \rightarrow 17/2^+$	0.25 *8*

1) The reduced transition probability was calculated according to the formula

$$B(M1) = 5.61 \times 10^{-4}\, P\, E^3\, \tau[\mu_N^2]$$

The mentioned above collective properties do emerge, as we have shown [18], from the large scale shell-model calculations. We have demonstrated that both the B(M1) and the B(E2) values are fairly well reproduced for the positive parity bands in ^{45}Sc (see also Tables 4 and 5 below).

On the very same footing we have also calculated the negative parity states in all three studied nuclei i.e. ^{43}Ca, ^{45}Sc and ^{45}Ti. (The preliminary results were given in our previous short conference contributions [16,17].) In Fig. 14 we give details of the shell model calculations with the FPD6 effective empirical two-body interactions by Richter et al. [29] and allowing the protons and the neutrons to the full fp configuration space with the inclusion of the $0f_{7/2}$, $0f_{5/2}$, $1p_{3/2}$, $1p_{1/2}$ orbits. The effective proton and neutron charges were again kept the same as for the positive parity state calculations i.e. $e_p = 1.33\,e$ and $e_n = 0.64\,e$ which have been determined from E2 transition rates and quadrupole moments in light fp-shell nuclei [30]. Similarly as in the previous calculations the free-nucleon g-factors were assumed.

In Fig. 15 the reduced transition rates B(M1) and B(E2) which were calculated with the above shell model parameters are compared with the experimental values listed in Tables 6 and 7. A good overall agreement between both sets of the data can be noticed.

The strong competition between E2 and M1 transitions depopulating positive parity states in the nuclei under study (Table 5) might resemble the effect of shears mode excitation [31] discussed recently for heavier nuclei. However, this effect is encountered for by the exact shell model treatment [18] which proves to be possible for the lighter nuclei while very difficult for heavier ones.

In summary, the odd-A $f_{7/2}$ shell nuclei exhibit collective properties besides spherical structures. Both can be explained when using appropriate empirical effective interactions and the extended fp configuration space with the inclusion of the sd-fp cross-shell excitations.

The "termination" of the positive parity band in ^{45}Sc my be due to the full alignment of the fp protons and neutrons and the $d_{3/2}$ proton hole. It may also be due to the insufficiency of the experiment, e.g. in the case of ^{45}Ti the $3/2^+$ band terminates as low as at $19/2^+$. We do hope that the forthcoming experiments will elucidate more on this interesting question.

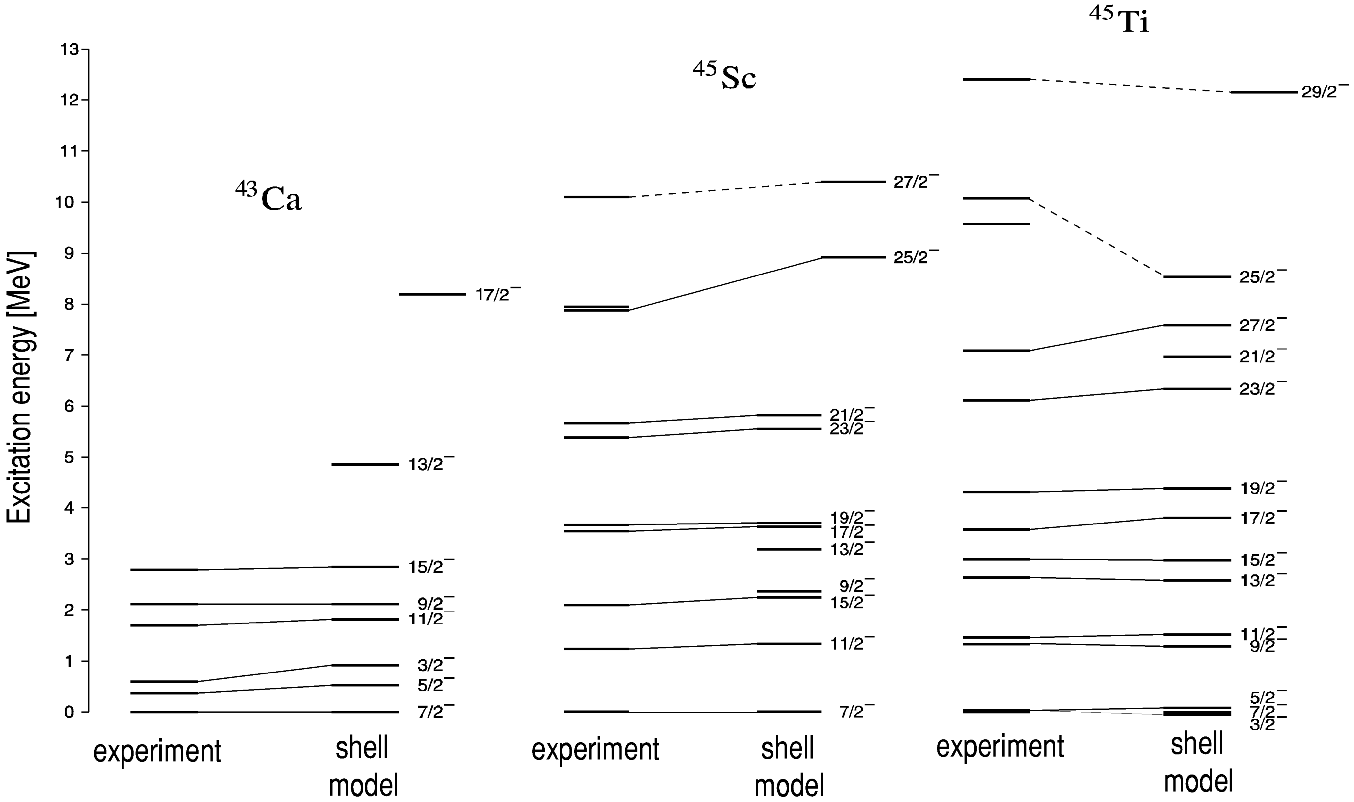

Fig. 14. Comparison between measured and calculated excitation energies of the negative parity states in ^{43}Ca, ^{45}Sc and ^{45}Ti. The levels with $J < J_{max}$ ($f_{7/2}$) result mainly from the $f_{7/2}$ excitations whereas the wave functions of the higher spin shell-model states (shifted to the right) involve the full fp-shell

Table 6. Experimental B(M1) transition rates deduced for the negative parity levels in ^{45}Sc (a) and ^{45}Ti (b)

E_γ [keV]	$I_i^\pi \rightarrow I_f^\pi$	$B(M1)_{exp}$ $^{1)}$ $[\mu_N^2]$
(a)	^{45}Sc	
1463	$17/2^- \rightarrow 15/2^-$	>0.18
123	$19/2^- \rightarrow 17/2^-$	2.0 4
2015	$21/2^- \rightarrow 19/2^-$	>0.27
2510	$25/2^- \rightarrow 23/2^-$	>0.05
(b)	^{45}Ti	
1188	$13/2^- \rightarrow 11/2^-$	>0.127
358	$15/2^- \rightarrow 13/2^-$	0.24 *9*
587	$17/2^- \rightarrow 15/2^-$	0.18 *3*
743	$19/2^- \rightarrow 17/2^-$	0.9 *2*

1) The reduced transition probability was calculated according to the formula

$$B(M1) = 5.61 \times 10^{-4}\, P\, E^3\, \tau\, [\mu_N^2]$$

Table 7. Experimental B(E2) transition rates deduced for the negative parity levels in ^{45}Sc (a) and ^{45}Ti (b)

E_γ [keV]	$I_i^\pi \rightarrow I_f^\pi$	$B(E2)_{exp}$ $^{1)}$ $[e^2fm^4]$
(a)	^{45}Sc	
1237	$11/2^- \rightarrow 7/2^-$	108 *6*
870	$15/2^- \rightarrow 11/2^-$	<818
1586	$19/2^- \rightarrow 15/2^-$	35 *7*
1725	$23/2^- \rightarrow 19/2^-$	28 *3*
(b)	^{45}Ti	
1468	$11/2^- \rightarrow 7/2^-$	171 *40*
1547	$15/2^- \rightarrow 11/2^-$	97 *34*
946	$17/2^- \rightarrow 13/2^-$	149 *26*
1330	$19/2^- \rightarrow 15/2^-$	<26
1818	$23/2^- \rightarrow 19/2^-$	82 *10*
981	$27/2^- \rightarrow 23/2^-$	60 *8*

1) The reduced transition probability was calculated according to the formula

$$B(E2) = 8.16\, P\, E^5\, \tau\, [e^2 fm^4]$$

The authors wish to thank W. Nazarewicz, E.Ormand and W. Satuła for stimulating discussions and their involvement in the theoretical interpretation of the results.

The studies reported in the article were supported in part by the Polish Committee for Scientific Research under Contract No. 2 P03B 112 08.

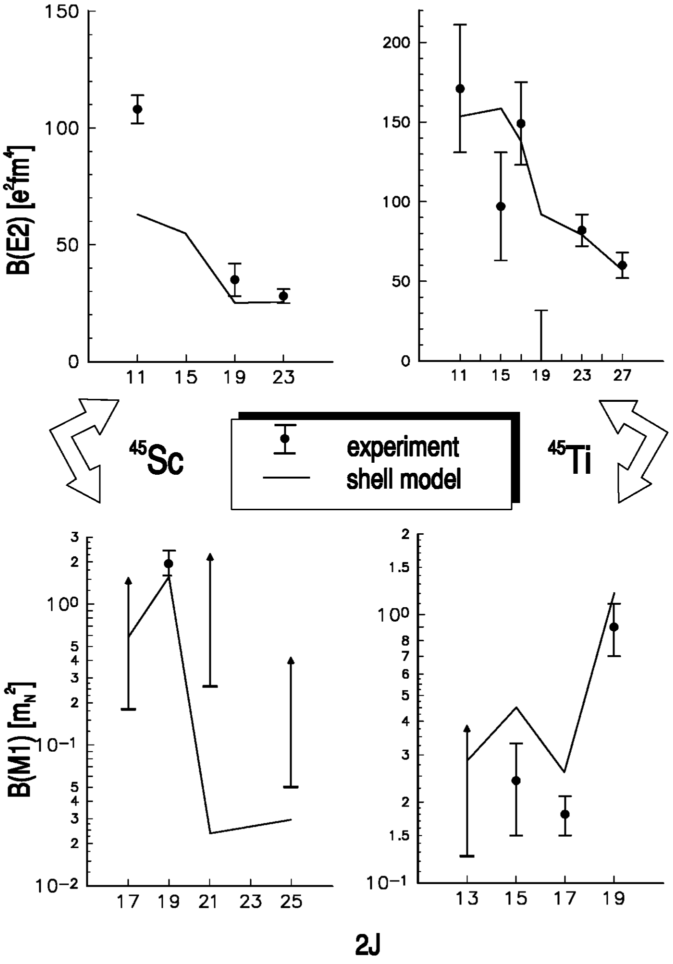

Fig. 15. Measured and calculated transition rates obtained for the negative parity levels in ^{45}Sc and ^{45}Ti

References

1. J. Kownacki, L. Harms-Ringdahl, J. Sztarkier, Z.P. Sawa, Phys. Script. **8**, 135 (1973)
2. B. Haas, P. Taras, J. Styczeń, Nucl. Phys. A**246**, 141 (1975)
3. J. Styczeń, J. Chevallier, B. Haas, N. Schulz, P. Taras, N. Toulemonde, Nucl. Phys. A**262**, 317 (1976)
4. G. Fortuna, S. Lunardi, M. Morando, C. Signorini, Nucl. Phys. A**299**, 479 (1978)
5. A.H. Behbehani, A.M. Al-Naser, A.J. Brown, L.L. Green, A.N. James C.J. Lister, N.R.F. Rammo, J.F. Sharpey-Schafer, L.H. Zybert, R. Zybert, P.J. Nolan, J. Phys. G. Nucl. Phys **5**, 1117 (1979)
6. P.G. Bizzeti, A.M. Bizzeti-Sona, M. Bucciolini, R. Huber, W. Kutschera, H. Morinaga, R.A. Ricci, C. Signorini, Nuovo Cim. **26**A, 25 (1975)
7. J. Kasagi, K. Itoh, T. Kishimoto, M. Sasaki, H. Ohnuma, Nucl. Phys. A**414**, 206 (1984)
8. D.K. Avasthi, K.C. Jain, I.M. Govil, V.K. Mittal, Act. Phys. Pol. B**16**, 847 (1985)
9. S.M. Lenzi, D.R. Napoli. A. Gadea, M.A. Cardona, D. Hojman, M.A. Nagarajan, C. Rossi Alvarez, N.H. Medina, G. de Angelis, D. Bazzacco, M.E. Debray, M. de Poli, S. Lunardi, D. Acuna, Z.Phys. A**345**, 117 (1996)
10. R.B.M. Mooy, P.W.M. Glaudemans, Z. Phys A**312**, 59 (1983)
11. E. Caurier, A.P. Zuker, A. Poves, G. Martinez-Pinedo, Phys. Rev. C**50**, 225 (1994)
12. E.K. Warburton, J.A. Becker, B.A. Brown, Phys. Rev. C**41**, 1147 (1990)
13. J.A. Cameron, D.G. Popescu, J.C. Waddington, Phys. Rev. C**44**, 2358 (1991)
14. S. Lenzi, C.A. Ur, D.R. Napoli, M.A. Nagarajan, D. Bazzacco, D.M. Brink, M.A. Cardona, G.de Angelis, M. de Poli, A. Gadea, D. Hojman, S. Lunardi, N.H. Medina, C. Rossi Alvarez, Phys. Rev. C**56**, 1313 (1997)
15. P. Bednarczyk J. Styczeń, R. Broda, M. Lach, W. Męczyński, INP, Annual Report 1991 (IFJ, 1992)
16. P. Bednarczyk J. Styczeń, R. Broda, M. Lach, W. Męczyński, D. Bazzacco, F. Brandolini, G. de Angelis, S. Lunardi, L. Müller, N. Medina, C. Petrache, C. Rossi-Alvarez, F. Scarlassara, G.F. Segato, C. Signorini, F. Soramel, Nucl. Phys. A**583**, 227 (1995)
17. P. Bednarczyk, R. Broda, M. Lach, W. Męczyński, J. Styczeń, D. Bazzacco, F. Brandolini, G. de Angelis, S. Lunardi, L. Müller, N. Medina, C. Petrache, C. Rossi-Alvarez, F. Scarlassara, G.F. Segato, C. Signorini, F. Soramel, W. Nazarewicz, E. Ormand, Acta Phys. Pol. B**27**, 145 (1996)
18. P. Bednarczyk, J. Styczeń, R. Broda, M. Lach, W. Męczyński, W. Nazarewicz, E. Ormand, W. Satuła, D. Bazzacco, F. Brandolini, G. de Angelis, S. Lunardi, L. Müller, N.H. Medina, C.M. Petrache, C. Rossi Alvarez, F. Scarlassara, G.F. Segato, C. Signorini, F. Soramel, Phys. Lett. B**393**, 285 (1997)
19. P. Spolaore, J.D. Larson, C. Signorini, S. Beghini, X. Zhu, H. Si, Nucl. Instr. and Meth. A**238**, 381 (1985)
20. F. Puhlhofer, Nucl. Phys. A**280** (1977) 267
21. D. Bazzacco, Proc. of International Conference on Nuclear Structure at High Angular Momentum, (Ottawa, 1992)
22. P. Spolaore, D. Ackermann, P. Bednarczyk, G. de Angelis, D.R. Napoli, C. Rossi-Alvarez, D. Bazzacco, R. Burch, L. Müller, G.F. Segato, F. Scarlassara, Nucl. Instr. and Meth. A**359**, 500 (1995)
23. A. Kramer-Flecken, T. Morek, R.M. Lieder, W. Gast, G. Hebbinghaus, H.M. Jager, W. Urban, Nucl. Instr. and Meth. A**275**, 333 (1989)
24. K.S. Krane, R.M. Steffen, R.M. Wheeler, Nuclear Data Tables **11**, 351 (1973)
25. T.K. Alexander, J.S. Forster, Advances In Nuclear Physics **10**, 197 (1978)
26. J.F. Ziegler, J.P. Biersak, V. Littmark The Stopping Power and Range of Ions in Solid (Pergamon Press, New York, 1985) Vol. 1.
27. T.W. Burrows, Nucl. Data Sheets **65**, 1 (1992)
28. W. Satuła, R. Wyss, and P. Magierski, Nucl. Phys. A**578**, 45 (1994)
29. W.A. Richter, M.G. Van der Merve, R.E. Julies, B.A. Brown, Nucl. Phys. A**523** (1991) 325
30. W.A. Richter, M.G. Van der Merve, R.E. Julies, B.A. Brown, Nucl. Phys. A**577** (1994) 585
31. G. Baldsiefen, H. Hübel, W. Korten, D. Mehta, N. Nenoff, B.V. Thirumala Rao, P. Willsau, H. Grawe, J. Heese, H. Kluge, K.H. Maier, R. Schubart, S. Frauendorf, H.J. Maier, Nucl. Phys. A**574**, 521 (1994)